APPLICATIONS OF RAMAN SPECTROSCOPY ON DEVELOPMENT OF SOLAR CELLS

Dr. Nandini Gattadahalli
Affiliation: Assistant Professor
Department of Humanities and Applied Sciences
New Horizon Institute of Technology and Management
Anand Nagar, Thane West, Maharashtra -400615, INDIA
Email id: gnpranav1970@gmail.com

Abstract— *Solar cells are one of the major alternative energy resources to fossil fuels. Solar cells are manufactured using materials such as silicon, hybrid Perovskites, and copper-zinc-tin-sulphides (CZTS), among others. Raman Spectroscopy is a branch of vibrational spectroscopy that acts as a supporting tool to X-ray diffraction in understanding the structure and composition of materials. Raman Spectroscopy is extensively used to study the crystalline nature of silicon, the degradation of hybrid Perovskites, and the formation of secondary phases in Kesterite semiconductors, among other applications. Raman spectroscopy is one of the most effective methods for detecting the optimal performance of solar cells. The present article is a Literature Survey on Applications of Raman spectroscopy in the development of solar cells.*

Index Terms— Raman Spectroscopy, Silicon Solar cells, Hybrid Perovskite, Formamidinium Lead Iodide, Methylammonium Lead Iodide, Tandem Solar cells.

I. INTRODUCTION

Solar energy is a crucial renewable energy source. Solar energy is a component of photosynthesis, photo electrochemistry, and other related processes. A photovoltaic (PV) cell, commonly referred to as a solar cell, is a non-mechanical device that converts sunlight directly into electricity [1]. Solar cells are classified based on their chemical composition. They include silicon solar cells, hybrid Perovskite solar cells, dye-sensitized solar cells, Tandem solar cells, etc [1].

The property of any solar cell is the transparency of its surface, high absorption, and low reflection of sunlight. The chemical constituents forming a solar cell should not decompose when exposed to extreme temperatures (0 °C to 50°C above) and atmospheric conditions, such as the presence of moisture or dry weather, for a long time [1].

Silicon is an inorganic element. Silicon is a semiconductor. Silicon is quite stable at high and low temperatures, rainy seasons, and dry climates. Silicon exhibits high transparency, high absorption, and low reflectivity of sunlight. Silicon (Si) is the first material used for the manufacture of solar cells. Silicon solar cells are extensively used. The power conversion efficiency (PCE) of a solar PV cell is expressed as the percentage ratio of electrical power produced to optical power impinging on the cell [1]. The maximum power conversion efficiency (PCE) of silicon solar cells is 30%. Figure 1 gives the impression of a typical crystalline solar cell. Advanced material research is providing better solar cells with PCE beyond 30% [1, 2].

Perovskite material is called Calcium Titanate ($CaTiO_3$) discovered by Mr. Gustav Rose at Ural Mountains in Russia in 1839 [3]. Mr. Gustav Rose named Calcium Titanate mineral after Russian Mineralogist Lev Perovski (1792-1856) as Perovskite mineral [3]. Perovskite mineral is an inorganic compound. Hybrid Perovskite materials have the generic form ABX_3. Hybrid Perovskite materials have the same crystallographic form as the Perovskite mineral Calcium Titanate [3, 4]. Hybrid Perovskite materials (ABX_3) contain inorganic and organic cations [4]. A is an organic cation composed of Formamidinium (FA), $(CH_5N_2)^+$, Methylammonium (MA), $(CH_3NH_3)^+$. B is a divalent inorganic cation like lead (Pb). X is a negatively charged anion containing halides [4]. Hybrid Perovskite materials show characteristic properties of solar cells like high absorption and low reflection [4]. The PCE of hybrid Perovskite solar cells is 30-45% [4]. Hybrid Perovskite materials have their own disadvantages. Hybrid Perovskite materials decompose at high temperature and in the presence of moisture [4]. During the processing of hybrid Perovskite

solar cells, Lead (Pb) leads to toxicity. Hybrid Perovskite solar cells are not yet commercialized. Figure 2 represents a unit cell of the Perovskite molecule [3-4]. Figure 3 is a representation of Perovskite solar cells [5].

Figure 1: Crystalline silicon solar cell [1]

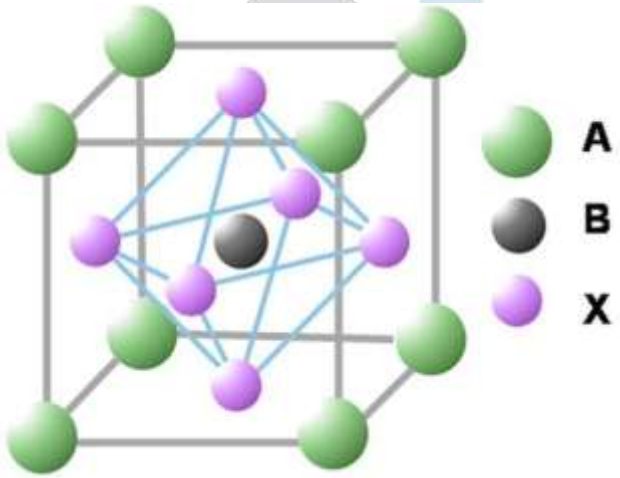

Figure 2: Unit cell of a ABX_3 Perovskite. In Hybrid Perovskites, A is an organic cation representing either Formidinium (FA) or Methylammonium (MA) cation, B represents divalent or tetravalent metal like Pb or Sn, X represents halides like I or Br or Cl. [permission from Reference (4)]

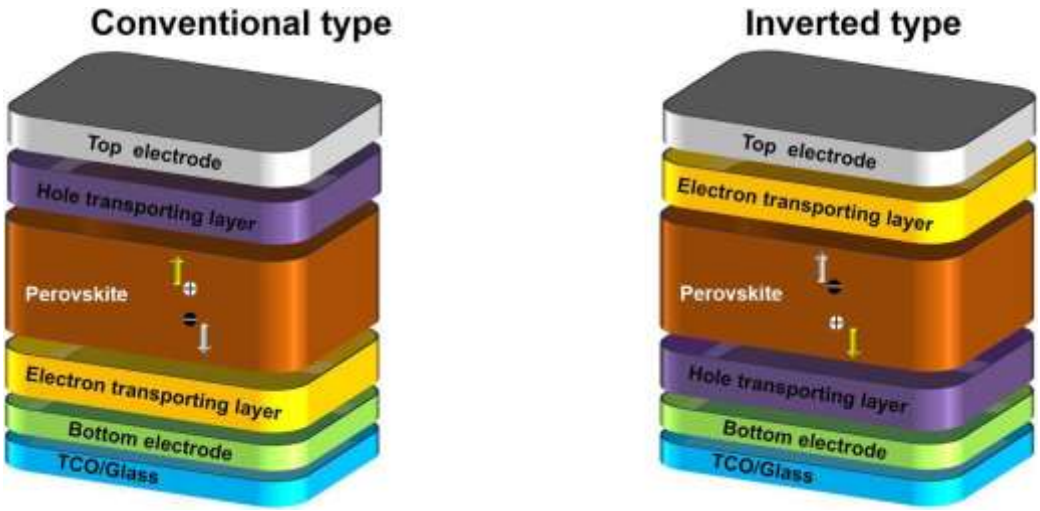

Figure 3: Two general device structures of Perovskite solar cells [Permission from Ref. (5)]

Dye-sensitized solar Cells (DSSC) are devices that convert the visible wavelength band of light to electrical energy [6]. The main component in DSSC is the Dye sensitizer [6]. Other components of DSSC are glass substrate, transparent conducting layer, TiO_2 nanoparticles, dyes, electrolyte (I^-/I_3^-), and counter electrode [6]. The main disadvantage of DSSC is dye sensitizer materials

decompose at high temperatures [6]. DSSCs are not commercialized. The PCE of DSSC is not beyond 25% [6]. Figure 4 is a representation of part of a DSSC solar cell.

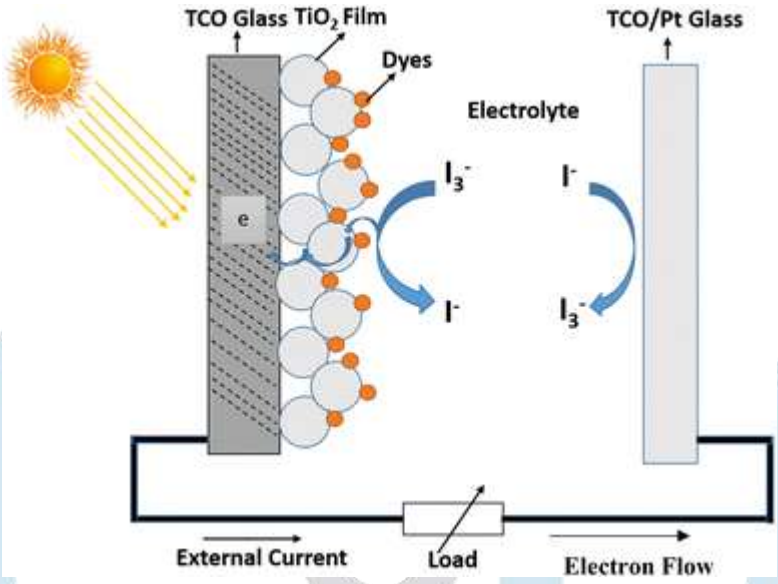

Figure 4: Diagram representing the layout and functioning of the DSSC. [Permission from Ref (6)]

Kesterite copper zinc tin chalcogenides, specifically Cu_2ZnSnS_4 (CZTS) (copper zinc tin sulphide) and $Cu_2ZnSnSe_4$ (CZTSe) (copper zinc tin sulphide-selenide) are used as absorber materials in thin-film photovoltaics (PV) [7,8]. Main advantages of CZTS are low cost and non-polluting nature [7,8]. CZTS has an optimal bandgap of 1.5 eV [7,8]. The optical absorption coefficient of CZTS is 10^4 cm^{-1} in the visible region [7,8]. Actual PCE has an approximate value of 12.6% [7,8]. Copper Zinc Tin Sulphide (CZTS) is a good alternative to copper indium gallium selenide (CIGS) as absorber materials in solar cells [7,8]. The disadvantages of CZTS are low PCE and formation of secondary phases [7,8]. Figure 5 is a representation of the CZTS solar cell [8].

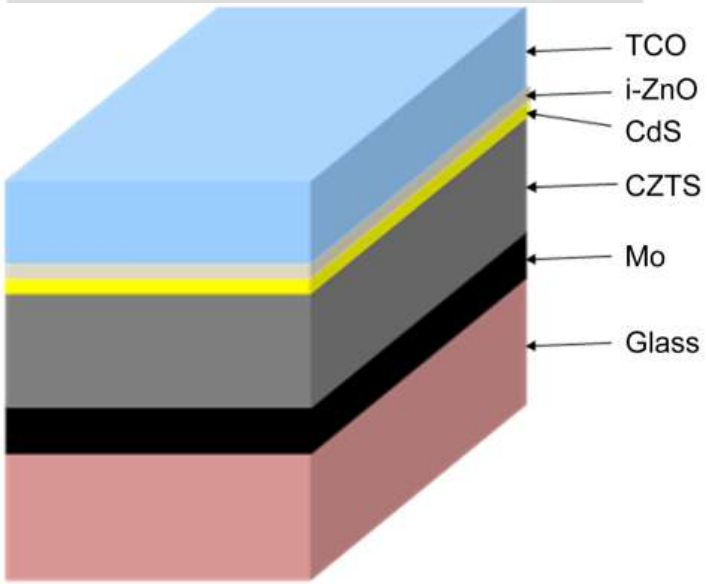

Figure 5: CZTS solar cell, a schematic structure [Permission from Ref (8)]

Tandem Solar cells are a new technical innovation to improve the PCE of solar cells [9]. Tandem solar cells are a combination of hybrid Perovskite solar cells with silicon solar cells, Hybrid Perovskite solar cells with CIGS (Copper Indium Gallium Selenium) cells, etc [9]. This combination has the advantage of the strength of both materials and provides higher PCE than individual solar cells [9].

Figure 6 is a representation of a sample of a Tandem solar cell. It consists of a hybrid Perovskite material at the top layer absorbing visible wavelength of sunlight and the bottom layer consists of a silicon solar cell absorbing Infrared Red (IR) wavelength of sunlight [9,10]. This kind of arrangement will increase the PCE of the solar cell [9,10].

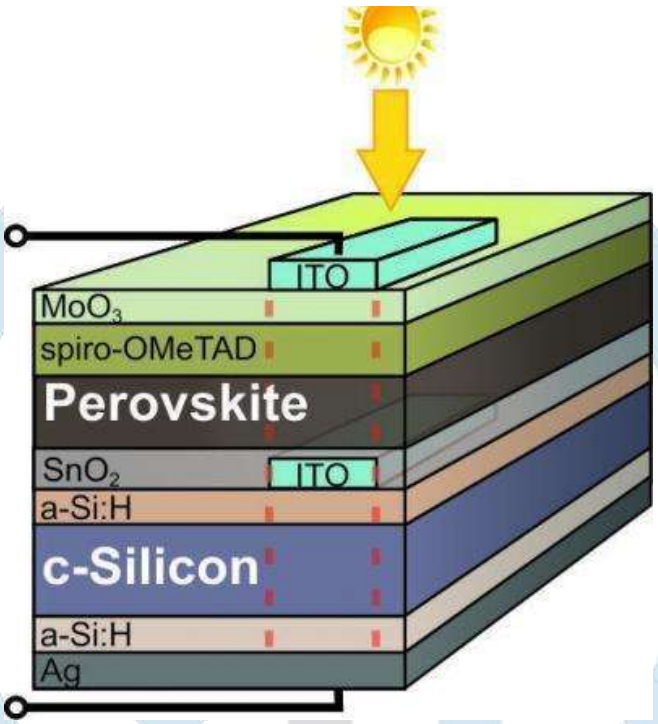

Figure 6: Schematic representation of a Tandem solar cell [Ref:10]

X-ray Diffraction (XRD), Infrared spectroscopy (IR), Raman Spectroscopy, UV-Visible spectroscopy (UV), Scanning Electron microscopy (SEM), Transmission electron microscopy (TEM), etc [11] are analytical techniques used to detect defects in structure, presence of impurities, stability of solar cells, etc [11]. Raman spectroscopy analyses crystallinity of various types of silicon, stability of hybrid Perovskite and absorber materials [9,11,12]. Raman spectroscopy as a characterization technique provides extensive support to data obtained by the X-ray diffraction method [11,29].

The present chapter is a literature survey on the application of Raman spectroscopy in the development of solar cells [1-39]. The present chapter will explore the specific applications of Raman spectroscopy in understanding the crystal structure of materials used in solar cells, defects in crystal structure, decomposition of materials, and stress measurement in solar cell thin films [1-39].

2. Basics of Raman spectroscopy

Raman Spectroscopy and Infrared spectroscopy are two branches of Vibrational spectroscopy. The Raman spectrum is observed due to a change in the polarizability of molecules; the IR spectrum is observed due to a change in the dipole moment of a molecule [13].

What is Raman scattering?

When light falls on a molecule, most of the energy is scattered without a change in its original value. This kind of scattering is called Elastic scattering or Rayleigh scattering. Some light scattered from a molecule will have a change in Energy E-ΔE. This kind of scattering is called inelastic scattering or Raman scattering. A small change in scattered energy is 1/100000000 of the original energy. This small change in scattered energy was discovered by Sir C.V. Raman [13,14]. Sir C.V. Raman was awarded the Nobel Prize in 1930 for the discovery of the Raman effect [13, 14]. The scattered photon with a lower frequency than the original photon gives a spectral line called as Stokes line. The scattered photon with a higher frequency than the original photon is called as anti-Stokes line [13,14]. Figure 7 is a representation of Stokes, anti-Stokes, and Rayleigh scattering.

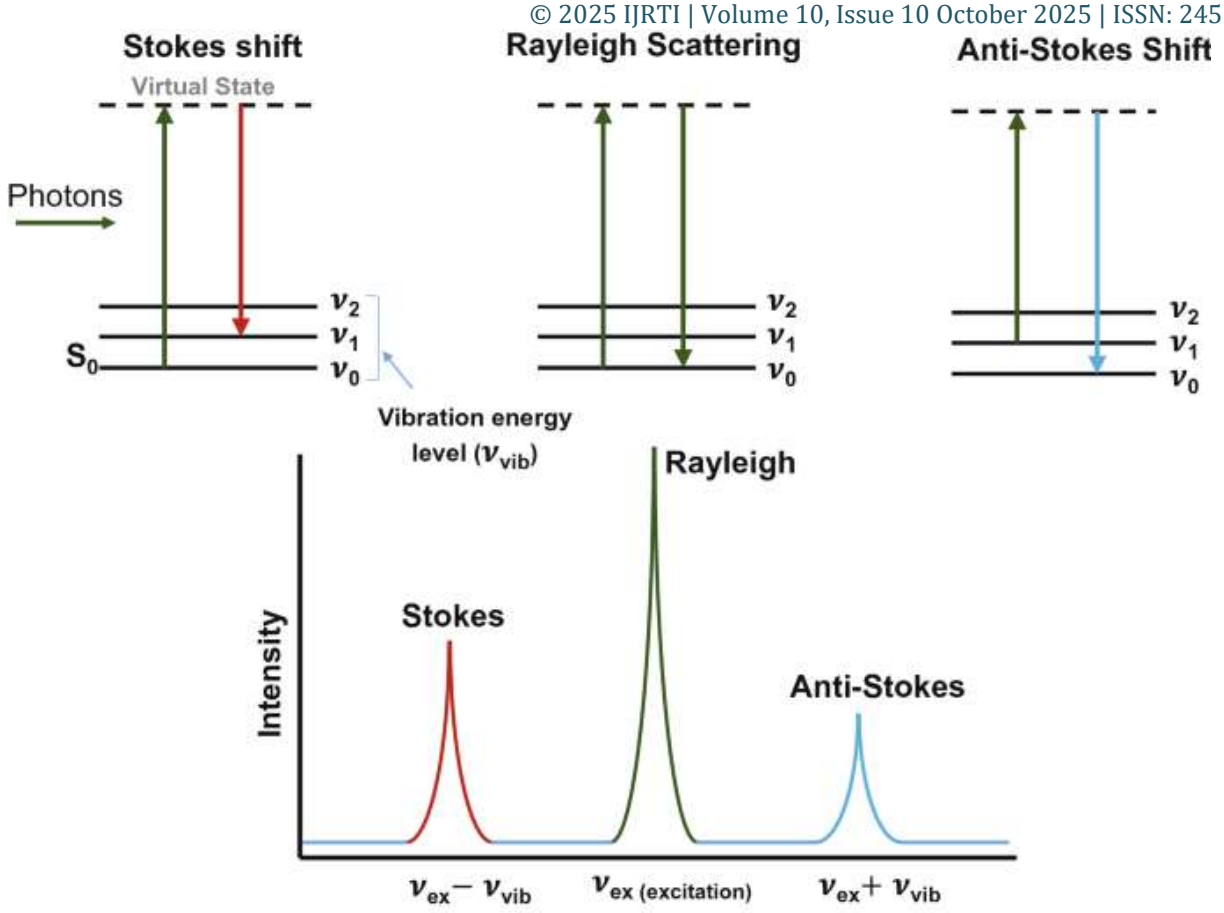

Figure 7: Representation of Rayleigh scattering, Stokes Raman and anti-Stokes Raman scattering. [permission from Ref:15]

Figure 8 represents the Raman spectrum of Anatase (TiO2), Stokes Raman scattering, anti-Stokes Raman scattering, and Rayleigh Scattering are shown in the given Raman spectra.

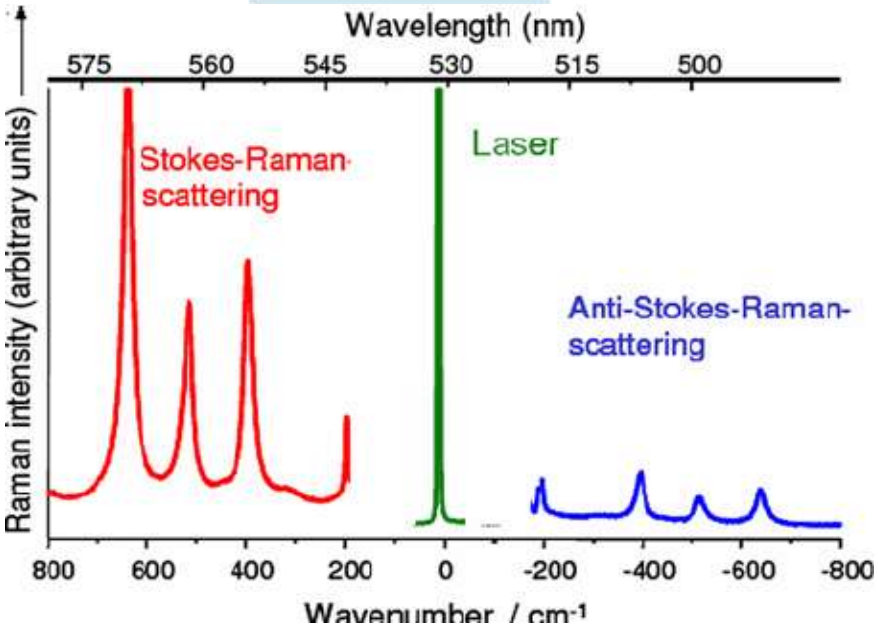

Figure 8: Stokes and anti-Stokes Raman spectra of anatase (TiO_2) [Permission from Ref 16]

Raman spectroscopy explains the shift of energy of the scattered photon in relation to the energy of the original photon [13,14]. The shift in energy of the scattered photon depends upon the chemical composition of the molecule [13,14]. The intensity of Raman scattering is proportional to the magnitude of the change in the molecular polarization [13,14]. Measured Raman signals are characteristic of every molecule [13,14].

Raman instruments are portable to given sites [17]. The signals are collected in a probe is connected to the detector and source, which is laser light of various wavelengths [17]. The laser wavelengths used influence the stability of materials [11,32-37]. Portable Raman instruments are extremely helpful in analysing various materials used for solar cells at reactive sites [17].

Different types of Raman spectroscopy listed below are extensively used in the development of solar cells.

a) Surface Enhanced Raman Spectroscopy (SERS) [11]
b) Resonance Raman Spectroscopy (RRS) [18]
c) Tip-enhanced Raman spectroscopy (TERS) [19]
d) Coherent anti-Stokes Raman spectroscopy (CARS) [20]
e) Micro- and Macro Raman Spectroscopy, etc [21].

In the next sections, applications of Raman spectroscopy in detecting crystallinity of silicon solar cells, decomposition of hybrid Perovskite Solar cells are discussed.

3. Applications of Raman spectroscopy to the development of silicon-based solar cells.

Different types of silicon are used in the manufacture of solar cells are listed below: They are

- Monocrystalline silicon
- Polycrystalline silicon
- Amorphous silicon.

The general definition of Crystallinity refers to the proportion of the crystalline regions within a material, describing the relative ratio of ordered crystal structures to disordered amorphous areas [12]. Crystallinity in solar cells is defined as the degree to which the semiconductor material (usually silicon) is arranged in a highly ordered, crystalline structure [12]. Higher crystallinity of silicon provides better performance; good crystal structure allows efficient electron flow and reduction in energy losses [12]. Higher crystallinity has very less defects and imperfections, no hindrance to electron movement. The higher crystallinity of silicon, better PCE of the silicon solar cell [12].

The normal mode of vibrations in the solid state is called Phonons [12]. These Phonons are detected by Raman spectroscopy [12]. Raman spectroscopy detects different vibrational modes or Phonons in crystalline and amorphous silicon, providing valuable crystallization information [12].

Droz et al [12] recorded Raman spectra for crystalline, polycrystalline, and amorphous silicon phases at 514nm and 633nm excitation light [12]. Crystalline silicon (monocrystalline or polycrystalline silicon) exhibits a sharp, high-intensity Raman peak around 520 cm^{-1} [12]. Amorphous silicon, due to its disordered structure, shows a broader spectral band near 480 cm^{-1} [12]. Additionally, microcrystalline silicon displays a characteristic peak around 510 cm^{-1}, which is broader than the crystalline silicon peak at 520 cm^{-1} [12]. The crystallinity of silicon material is quantified with intensity ratios of the peaks observed in crystalline, microcrystalline, and amorphous silicon [12]. Droz et al [12] evaluated the Raman crystallinity factor Φc using the intensity of the obtained Raman bands. The crystallinity factor Φc is 0.52 for high crystalline silicon and 0.28 for the amorphous phase at the excitation wavelength 514nm [12].

Sarau et al [21] utilized Micro- and Macro-Raman spectroscopy to detect stress, dislocation, and doping effects on silicon solar cells [21]. When external stress is applied to a silicon material, the phonon vibration frequency observed in Raman spectra changes due to a change in lattice constant [21]. Compressive stress shifts the Raman peak from 520 cm^{-1} to higher wave numbers while tensile stress shifts to lower wavenumbers [21]. This shift can be quantified to observe stress [21]. Figure 9 is a representation about tensile stress and compressive stress on a silicon solar cell and shifts in the Raman peaks based on the stress.

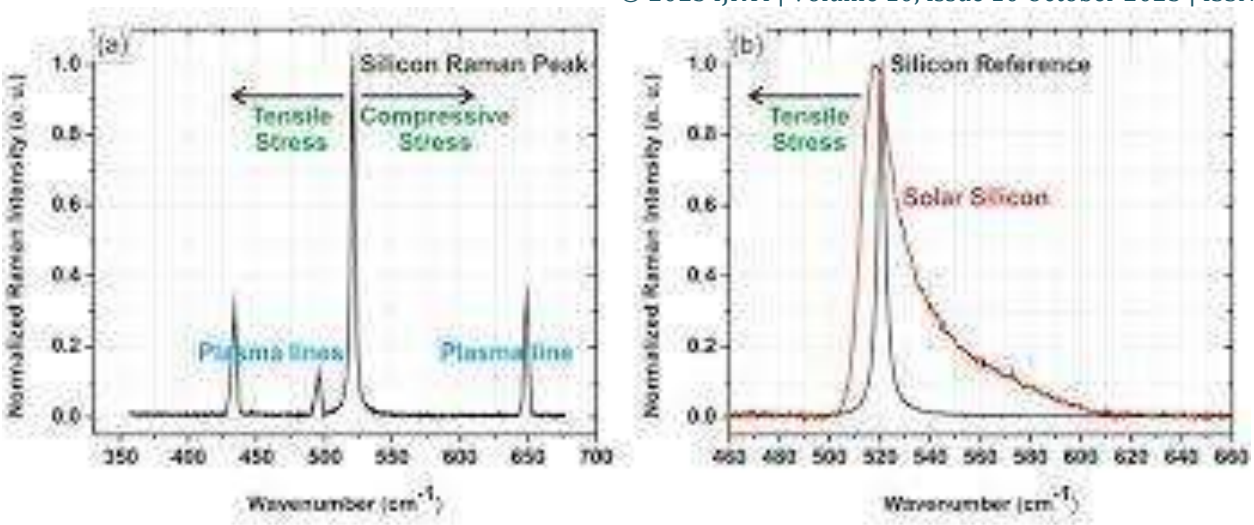

Figure 9:

a) The Raman spectrum of a silicon wafer is used as a reference. In the absence of stress, the three Raman optical phonons of Silicon are degenerate and give a single Raman Peak at ~520 cm^{-1}. Tensile stress or comprehensive stresses (internal or external) below 1GPa (Giga Pascal) may shift the Silicon Raman Peak to lower and higher frequencies, respectively. [Permission from Ref (21)

b) Comparison between Raman spectra of stress-free silicon wafer (reference material) and tensile-stressed thin film solar silicon on glass. Solar silicon is doped with boron so it shows an asymmetrical peak [Permission from Ref (21)]

Certain photovoltaic materials like CIGS (Copper Indium Gallium Selenide solar cells), CdTe (Cadmium Telluride) are deposited on heterogeneous substrates, which introduces certain stress. This residual stress is detected by Raman spectroscopy. This observation helps in proper deposition and improvement in material performance [22]. Raman spectroscopy plays a crucial role in the development of silicon solar cells to obtain better PCE. In the next section, the application of Raman spectroscopy in the development of hybrid Perovskite solar cells is discussed.

3. Applications of Raman Spectroscopy in the development of Hybrid Perovskite Solar Cells.

In the present section, the discussion is based on the application of Raman spectroscopy in the development of hybrid Perovskite solar cells.

Kim et al [23], Green et al [24] had done extensive studies on the growth of hybrid Perovskite materials into high-efficiency solar cells. Hybrid Perovskite materials are showing the greatest promise of PCE. Raman spectroscopy is playing a key role in understanding the structure of different hybrid Perovskites, their stability, and other properties [11]. Figure 10 is a representation of a Perovskite unit cell of different chemical composition.

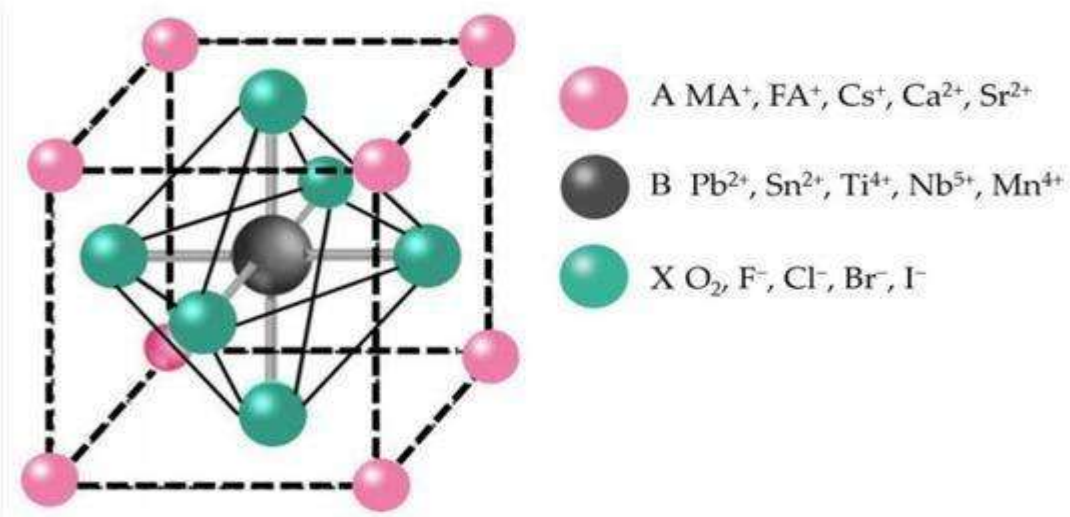

Figure 10: Perovskite Unit cell with proper chemical composition [Permission from Ref (25)].

Quarti et al [26] recorded and interpreted Raman spectra of hybrid Perovskite cells of type $MAPbI_3$ [MA methylammonium]. Quarti et al [26] measured the Raman spectrum for the $MAPbI_3$ film deposited on mesoporous Al_2O_3 under resonant conditions using an excitation wavelength of 532nm. The experimental frequency is shown in Figure 11(a). Quarti et al [26] identified three different types of periodic structures for hybrid Perovskite $MAPbI_3$. These periodic structures were labelled as tet-1, tet-2, and ortho, where tet-1 has a disordered tetragonal structure, tet-2 has an ordered tetragonal structure (head-to-tail structure) of four cations, and ortho has an orthorhombic structure (Pnma symmetry group) [26]. The geometry optimization and calculation of Raman spectra for tet-1, tet-2, and ortho structures were done using the Quantum Espresso Program package [26]. These theoretical calculations were conducted to support the experiments [26]. Calculated Raman frequencies for three periodic structures are represented in Figure 11(b, c, d) [26].

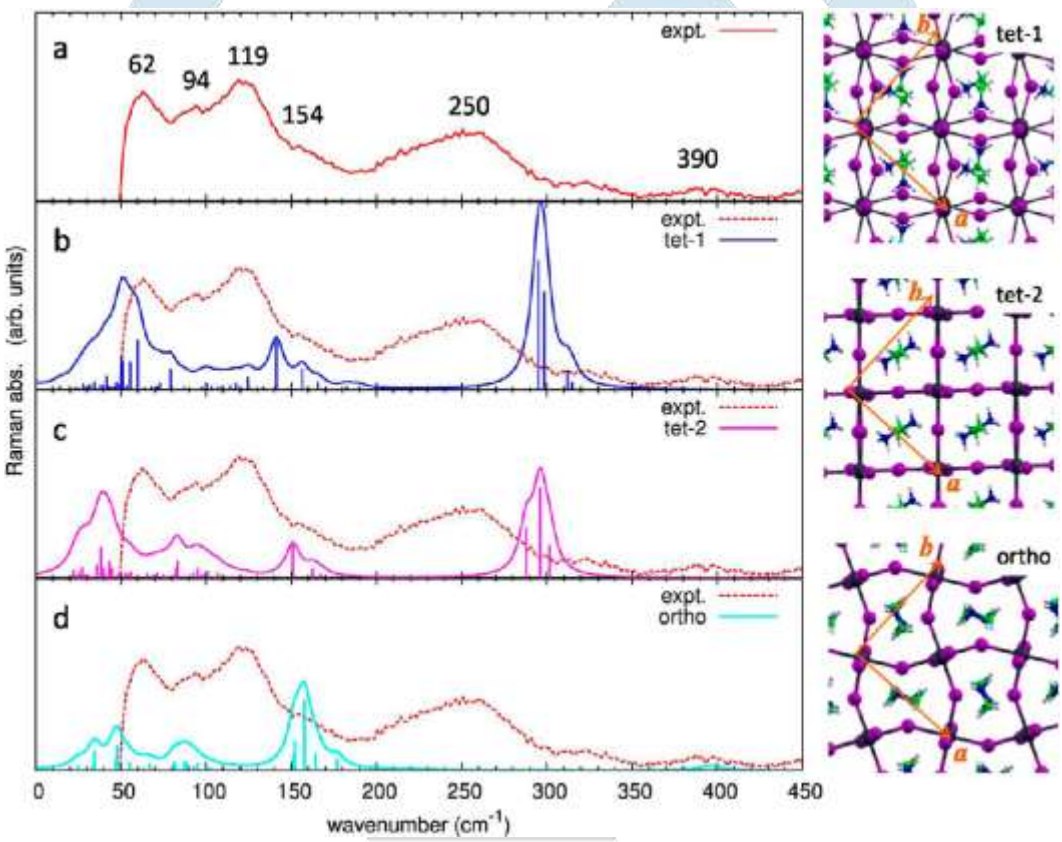

Figure 11: **Left: (a) Experimental resonant bands (b, c, d) nonresonant calculated for (tet-1, tet-2, ortho conformers) of $MAPbI_3$.[Permission from Ref (26)]**

Right: Optimized structures tet-1, tet-2, and ortho are shown on the right side. [Permission from Ref (26)]

Quarti et al [26] assigned;

- ~60 -64 cm^{-1} to I-Pb-I bending,
- ~94 cm^{-1} to Pb-I stretching,
- ~100-200 cm^{-1} to MA liberational modes and
- ~200-400 cm^{-1} to MA torsional modes.

Raman spectrum was calculated for isolated MA, isolated MA^{+3} Iodide ions, periodic structures of $MAPbI_3$, Raman modes were shifting to low wavenumbers in all three theoretical structures, shifting due to interaction between organic cation and inorganic group in hybrid Perovskites [26]. The isolated MA was showing wavenumbers of 465 to 490 cm^{-1}, whereas the periodic structure shifted to 295 to 399 cm^{-1} [26]. Torsional modes around 200-340 cm^{-1} are assigned to the organic group of hybrid Perovskites [26].

Nandi et al [27] used Raman spectroscopy and Photoluminescence spectra to investigate the structure of $CH_3NH_3PbI_3$ or $MAPbI_3$. Nandi et al [27] observed blueshift in the wavelengths of the Photoluminescence spectra of the sample with an increase in temperature. This is an indication of an increase in the band gap in the sample due to increased exciton-phonon interaction. Raman spectra for $CH_3NH_3PbI_3$ were recorded at room temperature (300K) [27]. Sharp Vibrational peaks were observed at 83.9 cm^{-1}, 136.3cm^{-1}, 274.8 cm^{-1} and broad peaks were observed at 350 cm^{-1}, 274.8 $cm^{-1,}$ and 350 cm^{-1} [27]. These spectra were confirmed with recordings done for the Tetragonal-1 structure, which has $(CH_3NH_3)^+$ (MA) as disordered packing [27]. Nandi et al [27] have done the assignment as follows:

- 83.9 cm^{-1} is assigned to Pb-I stretching,
- MA liberation modes at 136.3 cm^{-1},
- MA torsional modes at 274.8 cm^{-1},
- longitudinal optical modes (350 cm^{-1}) [27].

Ruan et al [28] studied Raman spectroscopy of Formamidinium (FA) based Perovskites $FAPbX_3$ (X=Cl, Br, I) and $FA_xMA_{1-x}PbI_3$ single crystals (MA: Methylammonium). Ruan et al [28] studied the Raman spectra of the transition change of $FAPbI_3$ to $FA_xMA_{1-x}PbI_3$ (replacement of FA cations by MA cations). When MA is replacing FA in the crystalline phase, MA shows ν(CN) at 955-958 cm^{-1}, FA shows ν(CN) at 1109 cm^{-1} [28]. MA shows ρ(NH_2) at 1465 cm^{-1}, FA shows ρ(NH_2) at 1382 cm^{-1} [28]. $FAPbI_xBr_yCl_z$ (where x,y,z=0,1,2,3) are other hybrid Perovskites that have similar properties to $FAPbI_3$. Ruan et al [28] recorded Raman spectra for various crystals of $FAPbI_xBr_yCl_z$ (where x,y,z=0,1,2,3), and a few normal modes of these crystals are presented in Table 1.

Table 1: Selected Raman Bands of $FAPbX_3$ [permission from Ref. (28)]

Materials	δ(NCN)	ν(CN)	ρ(NH_2)	δs(NH_2)	δ_{as} (NH_2)
$FAPbI_3$	516	1112	1380	1550	1613
$FAPbI_2Br$	517	1110	1385	1552	1615
$FAPbIBr_2$	519	1110	1386	1554	1618
FAPbBr3	520	1111	1389	1555	1620
$FAPbBr_2Cl$	521	1111	1390	1556	1623
$FAPbBrCl_2$	521	1111	1392	1556	1625
$FAPbCl_3$	522	1112	1393	1557	1627

δ for bending, s for symmetric, as for asymmetric, ν for stretching, ρ for rocking.

Gjoergjeviky et al [29] studied both X-ray diffraction data and Raman spectra for the following hybrid and inorganic Perovskites:

a) Methylammonium Lead Iodide ($MAPbI_3$),
b) Formamidinium Lead Iodide ($FAPbI_3$),
c) Cesium Lead Iodide ($CsPbI_3$),
d) Rubidium Lead Iodide ($RuPbI_3$),
e) Guanidinium Lead Iodide ($GUPbI_3$),
f) Dimethylammonium Lead Iodide ($DMAPbI_3$),
g) Pyrrolidinium Lead Iodide ($PYPbI_3$) crystals.

The Raman spectra for all the crystal structures were recorded using the Nd: YAG laser with an excitation wavelength of 632nm [29]. Normal coordinate analysis for every crystal was conducted [29]. Peaks below 200 cm^{-1} are considered for analysis [29]

According to Gjoergjeviky et al [29], the crystal structures of $MAPbI_3$ at room temperature, $FAPbI_3$ at low temperature have three-dimensional (3-D) structures. These 3-D structures do not have edge or face-sharing octahedra [29]. Two inorganic lead Perovskites ($RbPbI_3$ and $CsPbI_3$) as well as $GUPbI_3$, are one-dimensional (1-D) having edge-sharing octahedra [29]. One-dimensional structures do not have corner-sharing octahedra [29]. Gjoergjeviky et al [29] used Raman spectra of these crystals to understand the octahedral connectivity and dimensionality of these crystals.

Gjoergjeviky et al [29] divided Raman bands into three regions:

I. Internal vibrations of the inorganic Pb-I network frequencies are assigned between 10-50 cm^{-1}
II. Liberation and spinning of the organic cation (MA and FA) and the vibrations of the inorganic network (PbI_6) are coupled and assigned in the region 50-500cm^{-1}.
III. Organic cations like MA and FA have internal vibrations that are assigned above 500cm^{-1}. Inorganic lead iodides do not have Raman spectra beyond 300 cm^{-1}.

a) Polycrystalline $MAPbI_3$ has an orthorhombic phase at low temperature and has a three-dimensional corner-sharing octahedra. Gjoergieviky et al [29] recorded Raman spectra for Polycrystalline $MAPbI_3$. In the experimental Raman spectrum, the highest peak is observed between 90-100 cm^{-1}, the second (shoulder peak) at 110-120 cm^{-1}, and the third highest sharp peak at 60-70cm^{-1} [29]. The Pb-I modes show a blue shift compared to the Pb-I modes of pure PbI_2 crystal [29]. Gjoergieviky et al [29] conducted Normal coordinate analysis for Polycrystalline $MAPbI_3$. As per Normal coordinate analysis, Gjoergieviky et al [29] found 60 degrees of vibrational freedom, among them 24 are Raman active modes, 25 are IR active modes, 3 acoustic modes, and 8 silent modes. Raman active modes are $7A_g$, $5B_{1g}$, $7B_{2g}$, $5B_{3g}$ [29]. Gjoergieviky et al [29] assigned Raman modes as:

I. A_g symmetry mode as 108 cm^{-1} for Pb-I stretching, (Pure Pb-I in PbI_2 shows 94 cm^{-1}),
II. B_{2g} mode, B_{3g} mode are 56 cm^{-1}, 92 cm^{-1} for I-Pb-I bending respectively,
III. B_{1u} symmetry mode has a band at 69 cm^{-1} to I-Pb-I bending [29].

b) $FAPbI_3$ shows β-trigonal phase (P3) at low temperature and α-trigonal phase (P3m1) at high temperature. The difference between experimental Raman spectra of two crystalline phases is: at low temperature, the maximum peak is observed around 60-70cm^{-1}, and at high temperature, the maximum peak is around 90-100 cm^{-1}, the shoulder peak is around 110-120 cm^{-1}, the second largest peak is around 60-70cm^{-1} [29].

The third maximum peak is in the range 60-70 cm^{-1} at low temperature for $FAPbI_3$ and $MAPbI_3$, indicating vibrational modes of organic cations [29]. Normal coordinate analysis of the α-trigonal phase conducted by Gjoergieviky et al [29] gave 45 degrees of vibrational freedom, and the β-trigonal phase gave 180 degrees of freedom. All the modes are both IR and Raman active, predicting the absence of centre of symmetry for both β and α phases [29]. β-trigonal phase has 60A , 60E both are Raman and IR active, α-trigonal phase has 10A1, 15E modes both are Raman and IR active but 5A2 modes are silent [29]. Gjoergieviky et al [29] have done an assignment as follows:

I. A1 mode as Pb-I stretching at 110 cm^{-1}, 108 cm^{-1} for β, α phases, respectively.
II. E mode is I-Pb-I bending at 57 cm^{-1}, 56 cm^{-1} for β, α phases respectively as distorted stretching frequency [29].
III. Another degenerate E mode is Pb-I stretching at 93cm^{-1}, 92cm^{-1} for β, α phases respectively [29].

C and d) $CsPbI_3$ and $RbPbI_3$ are inorganic Perovskites. At room temperature, $CsPbI_3$ and $RbPbI_3$ have an orthorhombic (Pnma) crystal structure, having a dimensional structure with edge-sharing octahedra [29]. The experimental Raman spectrum for $CsPbI_3$ and $RbPbI_3$ shows the maximum intense peak at 100-110 cm^{-1} [29]. An intense peak is absent at 60-70cm^{-1} [29]. This confirms the observation that 60-70 cm^{-1} intense peaks may be assigned for organic cations [29]. Gjoergieviky et al [29] conducted normal coordinate analysis on $CsPbI_3$ and $RbPbI_3$. Normal coordinate analysis showed that both $CsPbI_3$ and $RbPbI_3$ have 60 degrees of vibrational freedom [29]. Among 60 degrees of vibrational freedom, only $10A_g$, $5B_{1g}$, $10B_{2g}$, $5B_{3g}$ are Raman active modes [29].

Gjoergieviky et al [29] assigned Raman Normal modes as follows:

I. Ag symmetry to the band 105 cm^{-1}, 107 cm^{-1} for $CsPbI_3$, $RbPbI_3$ as Pb-I stretching mode respectively;
II. B2g symmetry was assigned to the band at 112 cm^{-1}, 115 cm^{-1} as Pb-I stretching for $CsPbI_3$, $RbPbI_3$, respectively, as (with double octahedra expansion) mode;
III. Ag and B2g vibrational modes were assigned to the band at 93 cm^{-1}, 96 cm^{-1} for $CsPbI_3$, $RbPbI_3$, respectively.
IV. The bands above 80 cm^{-1} are assigned as Pb-I vibrations arising from equatorial double octahedral sharing;

V. The bands at 81 cm^{-1} and 52 cm^{-1} of $CsPbI_3$, 83 cm^{-1} and 56 cm^{-1} of $RbPbI_3$ are a combination of multiple vibrational modes,

VI. The bands at 52 cm^{-1}, 56 cm^{-1} are assigned as Cs-I, Rb-I vibrational modes, respectively.

VII. The band at 64 cm^{-1} for $CsPbI_3$, 67 cm^{-1} for $RbPbI_3$ is a combination of A_g, B_{1g} and B_{2g} vibrational modes [29].

e) The Guanidium lead iodide ($GUPbI_3$) (Pna21) is an orthorhombic crystal structure at room temperature [29]. At low temperature, $GUPbI_3$ has a monoclinic crystal phase (P21/c) [29]. For the orthorhombic phase of $GUPbI_3$ at room temperature, the experimental Raman spectrum shows a maximally intense peak from 90 to 100 cm^{-1} and shoulder peaks from 50-60 cm^{-1}, 60-70cm^{-1}, 100-120 cm^{-1} [29]. For the Monoclinic phase at low temperature, peaks from 50-60 cm^{-1}, 60-70cm^{-1}, 100-120 cm^{-1} are sharp, and the maximum peak is sharper than the orthorhombic phase at 90 to 100cm^{-1} [29]. Appearance of broad or sharp peaks from 60-70 cm^{-1} indicates the presence of an organic group [29]. Gjoergieviky et al [29] conducted Normal coordinate analysis on $GUPbI_3$ has 60 degrees of vibrational freedom. Among 60 degrees of vibrational freedom, $15A_1$, $15A_2$, $15B_1$, $15B_2$ modes are Raman active [29]. Gjoergieviky et al [29] assigned Raman Normal modes as follows:

I. A1, Ag symmetry mode is assigned at 105 cm^{-1}, 106 cm^{-1} for the orthorhombic phase, monoclinic phase as Pb-I stretching, respectively [29].

II. B_1, B_{1g} symmetry mode is assigned at 108cm^{-1}, 114 cm^{-1} for the orthorhombic phase, monoclinic phase as I-Pb-I bending mode, respectively [29].

III. B_2, B_{2g} is assigned at 55 cm^{-1}, 60 cm^{-1} for orthorhombic, monoclinic phase as I-Pb-I bending mode, respectively [29].

f) $DMAPbI_3$, $PYPbI_3$ are one-dimensional face-sharing organic-inorganic hybrid Perovskites [29]. At room temperature, they crystallize in the hexagonal crystal form(P63/mmc) [29]. The experimental Raman spectrum shows a shoulder peak at 60-80 cm^{-1} and a major intense peak at 100-110cm^{-1} peak [29]. Normal coordinate analysis of both the crystals produced 30 degrees of vibrational freedom [29]. Active Raman modes are: A_{1g}, A_{2g}, $2B_{2g}$, E_{1g}, $3E_{2g}$ [29]. Gjoergieviky et al [29] assigned Raman Normal modes as follows:

I. Eg symmetry mode is assigned at 56 cm^{-1}, 58 cm^{-1} for $DMAPbI_3$, $PYPbI_3$ to I-Pb-I bending respectively,

II. A_{1g} symmetry mode is assigned at 104 cm^{-1} for both $DMAPbI_3$, $PYPbI_3$ as Pb-I stretching mode [29].

Raman spectra of $MAPbI_3$, $FAPbI_3$, $GUPbI_3$, $CsPbI_3$, $RuPbI_3$, $DMAPbI_3$, and $PYPbI_3$ are overlapped, and correlation studies are done [29]. Four specific regions were identified as possible markers in the Pb-I network to determine octahedra connectivity [29]. They are 76 - 87 cm^{-1}, 92 - 96 cm^{-1}, 104 - 110 cm^{-1}, 108 - 116 cm^{-1} region in correlated Raman spectra [29].

i. At 76 - 87 cm^{-1}, edge-sharing structures exhibit blue shift (>80 cm^{-1}) and face and corner sharing octahedra show red shift (< 80 cm^{-1}) [29]. Edge-connected octahedra have steric hindrance, so blue shift, but face-sharing octahedra will have I-Pb-I vibrations (in plane) between two octahedra and give red shift [29].

ii. At 92 - 96 cm^{-1}, edge-sharing octahedral structures show this band, but face-sharing octahedral structures do not show this band [29]. Examples are $DMAPbI_3$, $PYPbI_3$ Perovskites [29].

iii. At 104-110 cm^{-1}, Pb-I stretching modes (A Symmetry) are shown in this region [29]. This band is observed when the number of sharing points between octahedra decreases due to steric hindrance [29]. The sharing points between octahedra decrease from face-centred octahedra to corner-sharing octahedral structures [29].

iv. At 108-116 cm^{-1}, I-Pb-I bending mode (B symmetry) is assigned, which is suitable for one-dimensional structures having edge-sharing octahedra [29]. Other crystal structures of Perovskites do not show this band [29].

Gjoergieviky et al [29] showed that Raman spectra of any new Perovskite crystal can be analysed easily. Gjoergjeviky et al [29] showed that Raman spectroscopy is one of the best support for the X-ray diffraction system to understand Perovskite solar cells.

This section provides a few discussions on understanding characteristic Raman spectra for hybrid Perovskites and inorganic Perovskites. This is required to understand the role of Raman spectroscopy in understanding the stability of Perovskites. The

Raman modes of Pb-I stretching, I-Pb-I bending in $MAPbI_3$, $FAPbI_3$, $CsPbI_3$, $RuPbI_3$, $GUPbI_3$, $DMAPbI_3$, $PyPbI_3$ are summarized in Table 2:

Table 2: Summary of Pb-I stretching mode and I-Pb-I bending mode, and MA liberation and torsion mode

Hybrid Perovskites	**Pb-I stretching in cm^{-1}: Pure Pb-I: 94 cm^{-1} [29]**		
	Quarti et al [26]	**Nandi et al [28]**	**Gjoergiviky et al[29]**
$MAPbI_3$	~94	83.9	Ag: 108
$FAPbI_3$			A1: 110 for β crystal phase A1:108 for α crystal phase E: 93 for β crystal phase E: 92 for α crystal phase
$GUPbI_3$			A1: 105: Orthorhombic Ag: 104: monoclinic
$DMAPbI_3$			A1g: 104
$PYPbI_3$			A1g: 104
Inorganic Perovskites			
$CsPbI_3$			Ag: 105, 93
$RuPbI_3$			Ag: 107, 96
Cs-I, Rb-I			52, 56
	I-Pb-I bending		
$MAPbI_3$	~60-64		B_{2g}:56 B_{3g}:92 B_{1u} : 69
$FAPbI_3$			E: 57: β phase E: 56: α phase
$GUPbI_3$			B_1:108: orthorhombic B2: 55: orthorhombic B_{1g} :114: monoclinic phase B_{2g} :60: monoclinic phase
$DMAPbI_3$			E_g : 56
$PYPbI_3$			E_g : 58
	MA liberational and torsional modes		
MA liberational modes	~100-200	136.3	
MA torsional modes.	~200-400	274.8	

Overall, Pb-I stretching is assigned at ~94-96 cm^{-1}, organic cations like FA, MA, vibrational modes assigned at ~60-70 cm^{-1} for hybrid Perovskites. This result is important to study the stability and degradation mechanism of Perovskites when exposed to laser excitation, moisture, and heat.

The next section is dedicated to understand the role of Raman spectroscopy in determining the stability of Perovskites.

4. Application of Raman Spectroscopy in determining stability and degradation of Perovskites

In the present section, Discussion is based on the influence of Raman spectroscopy in the quantitative determination of the degradation of hybrid Perovskite materials to PbI_2.

Shahbazi et al [30], reported that hybrid Perovskite [$MAPbI_3$] materials decompose when exposed to moisture and oxygen. $MAPbI_3$ degrades as follows [30]

$$CH_3NH_3PbI_3(s) \rightarrow CH_3NH_3I(aq) + PbI_2(s)$$

$$CH_3NH_3I(aq) \rightarrow CH_3NH_2(aq) + HI\ (aq)$$

$$4HI\ (aq) + O_2(g) \rightarrow 2I_2(s) + 2H_2O$$

$$2HI\ (aq) \rightarrow H_2O(g) + I_2(s)$$

$MAPbI_3$ decomposes to PbI_2. The performance of $MAPbI_3$ Perovskite solar cells is affected by their instability [30]. Hybrid Perovskites decompose to PbI_2 in the presence of moisture during structural elucidation by SEM, TEM, and XRD instruments [11]. Hybrid Perovskites decompose when exposed to excitation wavelengths beyond 632nm used in Raman spectroscopy [35].

Zhou et al [11] conducted real-time monitoring of Perovskite film stability using Raman spectroscopy to study the stability and decomposition of $MAPbI_3$ Perovskite films. Zhou et al [11] used Surface Enhanced Raman Spectroscopy (SERS) to study the crystallinity of $MAPbI_3$ Perovskite solar cells to understand the effect of crystallinity on PCE. Zhou et al [11] treated Perovskite films with different anti-solvents[*.] (different ratios of ethanol (C_2H_5OH) and chloroform ($CHCl_3$)) [*]{·Anti solvent crystallization is a separation technology that separates a solute from the solvent by the addition of another solvent, in which the solute is sparingly soluble [31])}. Copper(II)phthalocyanine (CuPc) as the probe molecule to study the SERS of Perovskite films. CuPc does not react with Perovskite films.

Zhou et al [11] treated $MAPbI_3$ Perovskite films having different crystallinities with antisolvents of ethanol (C_2H_5OH) and chloroform ($CHCl_3$) in different ratios. Anti-solvent treatment increases the Perovskite grain size and passivates defects at the interfaces of solar cells, and increases absorption of light. Zhou et al [11] measured absorption levels of anti-solvent-treated $MAPbI_3$ Perovskite films using UV-visible spectroscopy, level of crystallinity by X-ray diffraction, grain size of $MAPbI_3$ Perovskite films, homogeneity and pore size by Atomic force spectroscopy, recording Raman spectra with variation of time from 0 to 80 minutes, and measurement of PCE was done. The results are mentioned below:

- UV-Visible spectroscopy (from 600-900nm) was used on these $MAPbI_3$ Perovskite films to check the maximum absorption, and Zhou et al [11] found that Perovskite films treated with 1:4 C_2H_5OH and $CHCl_3$ show the highest absorbance (~0.30 absorbance measured in atomic units).
- Zhou et al [11] found that a volume ratio of 1:4 of C_2H_5OH and $CHCl_3$ provides the highest crystallinity for $MAPbI_3$ Perovskite films confirmed by X-ray diffraction study.
- Atomic force microscopy studies were conducted on untreated and anti-solvent-treated Perovskite films and found that the film that has been treated with 1:4 C_2H_5OH and $CHCl_3$ shows minimum roughness and pores [11].
- Scanning electron microscopy (SEM) are used to find the grain size of $MAPbI_3$ Perovskite films, and found those films treated with 1:4 C_2H_5OH and $CHCl_3$ have maximum grain size and homogeneity [11].
- Zhou et al [11] recorded Raman spectra in the presence of Nitrogen to avoid the exposure of $MAPbI_3$ Perovskite films to oxygen and water, so that it does not degrade. Monitoring of Raman signals was done in Real time, and time was varied from 0 to 80 minutes [11].
- The time-dependent plot of Raman intensities with temperature showed maximum intensity observed at peak 1528 cm^{-1} at 110°C and time varied from 0 to 10 minutes [11]. Excess heating with an increase in time intensity of Raman peak drops and shows Perovskite films are getting degraded [11]. Measured XRD intensities support Raman spectral data [11].
- The PCE of Perovskite films was measured for both untreated and anti-solvent treated Perovskite films [11] and found that $MAPbI_3$ Perovskite films treated with anti-solvent of ratio 1:4 C_2H_5OH and $CHCl_3$ provided PCE of 14% which is 72.8% higher than untreated films [11].

Zhou et al [11] showed that the higher the crystallinity of $MAPbI_3$ Perovskite films, the better the PCE of solar cells, and the stability of films are high.

Hooper et al [32] conducted Optical Imaging and Raman mapping[$] to tackle the challenge of probing degradation and homogeneity of Perovskite PV films within a photovoltaic device stack. The top and bottom layers of the Perovskite solar cell determine photo degradation. The amount of PbI_2 formed is estimated, and the distribution of PbI_2 in the entire solar cell with ~1 µm spatial resolution was done using Raman Mapping[$] [32]. Hooper et al [32] proved that Raman spectroscopy will be very useful to study other Perovskite semiconductor-based devices. Optical imaging was not successful in getting images of $MAPbI_3$ degradation to PbI_2, but Raman spectra observed $MAPbI_3$ decomposition to PbI_2 at 96cm^{-1} [32]. [$](Raman mapping, known as Raman imaging, is a chemical imaging technique that utilizes Raman spectroscopy to visualize the spatial distribution of

chemical and structural information within a sample. It works by scanning a laser beam across the sample and acquiring Raman spectra at various points, creating a chemical map that reveals the distribution of different components and their properties [33]).

Ghosh et al [34], reported the stability of hybrid Perovskite solar cells

- $FAPbBr_3$,
- $FAPbBr_3$.1Cl,
- $FAPbBr_3$.2Cl,
- $FAPbBr_3$.3Cl

where FA is organic cation (Formamidinum), Pb is Lead, Br is Bromine, Cl is Chlorine. Ghosh et al [34] utilized Raman spectroscopy to characterize the above compounds [34]. It was found that the compound with the highest Cl concentration shows better stability and an increase in the band gap of the solar cell [34]. Doping with Cl was changing the structure of hybrid Perovskite solar cell; the higher the doping of Cl, the higher the band gap [34]. X-ray diffraction analysis confirms the change in the crystal structure when the doping of Cl is increased in the $FAPbBr_3$ crystal. Experimental Raman Spectra and theoretical DFT calculations confirm the same results [34]. There was an absence of torsional NH_2 mode and asymmetric bending mode of NH_2 by $FAPbBr_3$.3Cl (band at 1620 cm^{-1} exhibited by $FAPbBr_3$, $FAPbBr_3Cl$) and presence of Hydrogen bonds between NH and halogens [34].

Pistor et al [35] developed a fast, contactless methodology to probe composition degradation of Perovskite solar cells. Pistor et al [35] showed the excitation wavelength of Raman spectroscopy done at 532nm and 633nm. Vibrational Properties of $MAPbI_3$(methylammonium lead iodide) thin films were extensively studied in both the wavelengths at 532nm and 633nm excitation [35]. The vibrational properties of PbI_2 molecules are reported. At higher excitation (633nm), there is a possibility of decomposition of $MAPbI_3$ to PbI_2. The experimental data were matched with theoretical data calculated using Density Functional Theory (DFT) [35]. Pistor et al [35] compared the obtained Raman peaks with those available in the literature [26]. The Raman spectra obtained from Pistor et al [35] and literature [26] did not have differences. Pistor et al [35] showed that Raman spectroscopy is best technique to monitor the degradation of Perovskite thin films in both excitation wavelengths [35] as depicted in Figure 12.

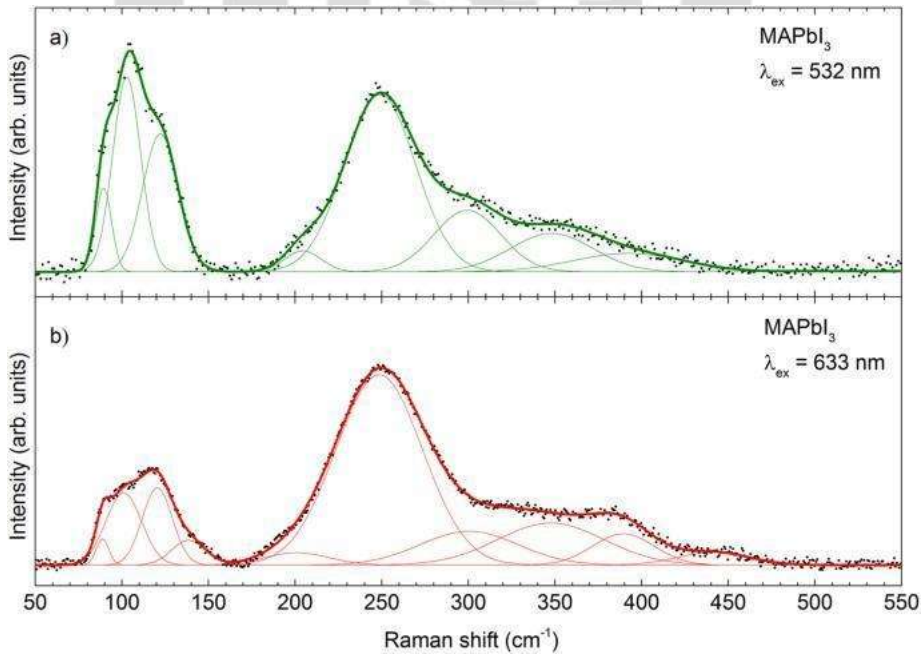

Figure 12: Raman spectra of $MAPbI_3$ thin films with excitation at (a) 532 nm and (b) 633 nm [Permission from Ref (35)]

In Figure 12, Raman peaks were sharp and precise when recorded at an excitation wavelength of 532nm compared to peaks recorded at an excitation wavelength of 633nm [35]. At 633nm, $MAPbI_3$ decomposes to PbI_2 [35].

Ledinsky et al [36] studied Micro Raman spectra of Pristine $CH_3NH_3PbI_3$, $CH_3NH_3PbBr_3$, and mixed iodide-bromide ($CH_3NH_3PbI_{3-x}Br_x$) thin films. Ledinsky et al [36] observed structural changes under 514.5 nm laser illumination and concluded that the cause of degradation is due to the formation of PbI_2 [36]. Due to laser illumination, it is observed that $CH_3NH_3PbBr_3$ degrades to $PbBr_2$ [36]. The disappearance of the Raman peak at 52 cm^{-1} and the appearance of an intense Raman Peak at 94 cm^{-1}

(pure PbI_2 shows an intense peak at 94cm^{-1}) provide a degradation mechanism for $CH_3NH_3PbI_3$ to PbI_2 [36]. An increase in doping of Br to $CH_3NH_3PbI_3$ forming mixed halide Perovskites $CH_3NH_3PbI_{x-1}Br_x$, the Raman spectra show a redshift compared to the Raman peaks of $CH_3NH_3PbI_3$ [36]. The redshift effect is used to estimate the Br-to-I ratio in mixed halide Perovskite films [36]. Ledinsky et al [36] used below notation to calculate the Br-to-I ratio:

$$P_{I+Br} = P_{Br}\,(1 - \alpha C_I)$$

Where C_I is the iodide concentration, P_{I+Br} **and** P_{Br} are Raman band positions of mixed Perovskites and pure $CH_3NH_3PbBr_3$. α is called the Raman shift coefficient and is equal to 0.31±0.31. Ledinsky et al [36] utilized Micro Raman spectroscopy to quantitatively measure the degradation of Perovskite films.

Gottesman et al [37] performed both theoretical and experimental studies on the performance of hybrid Perovskite cell $MAPbI_3$ (MA: methylammonium) in dark and light conditions. Gottesman et al [37] observed that $MAPbI_3$ undergoes structural modification under illumination. Structural modification of $MAPbI_3$ affects the efficiency of a solar cell. The crystal structure of $MAPbI_3$ differs in light compared to dark conditions [37]. $MAPbI_3$ has a better ordered crystal structure in light compared to the same crystal structure in dark conditions [37]. The Raman spectra of the crystal recorded in light conditions show sharper peaks compared to the Raman spectra of crystal recorded in dark conditions. These results were represented in Figure 13. Theoretical calculations confirm the same results [37].

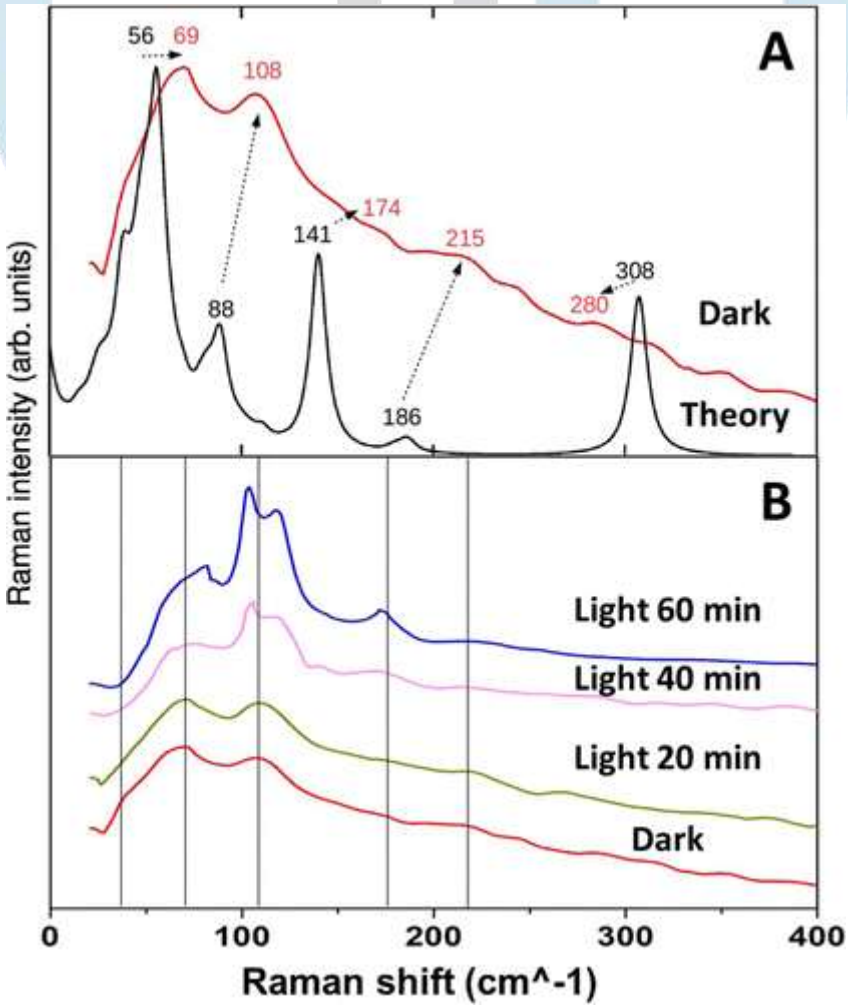

Figure 13: A) Experimental (taken in the dark) and theoretical Raman spectra of $MAPbI_3$ film, along with the main representative vibrational peaks [Permission from Ref. (37)]
B) Raman spectra for the same thin film taken in the dark and following illumination at 20, 40, 60 minutes, showing photoinduced structural changes of the $MAPbI_3$ [Permission from Ref. (37)]

Qiong Chen et al [38] studied photodegradation of Pristine $MAPbI_3$ at various stages and important Raman peaks are observed at various stages of degradation. The pure crystal $MAPbI_3$ was subjected to photo illumination and degradation of $MAPbI_3$ to PbI_2 was observed Raman and Photoluminescence spectra. Four stages were observed during the degradation of $MAPbI_3$ crystal and observed Raman spectra was represented in Table 3.

First stage is pure Pristine state of $MAPbI_3$, second stage is meta stable state, third stage is partially degraded state and fourth stage is fully degraded state

Table 3: Spectroscopic information on degradation stages of $MAPbI_3$ crystal. Reproduced with permission [38]

Stages	Raman peaks	Photoluminescence peaks
Pristine stage and stable state.	No visible discrete Raman modes around 100 cm^{-1} but with a broad band at ~550 cm^{-1}	
Metastable state	Appearance of a hump in the 100 cm^{-1} regions; reduction of the 550 cm^{-1} bands	Blueshift; peak intensity reduction; PbI_2 band edge PL peak appears at stage IV
Partially and irreversibly degraded state	Appearance of discrete Raman modes in the 100 cm^{-1} region, the 550 cm^{-1} band very weak	
Fully degraded state	Resembling PbI_2 Raman spectrum	

Many reports [11-38] suggest that the Perovskite films are an excellent model for solar cells. Raman spectroscopy (SERS, Micro- and Macro- Raman spectroscopy) are few excellent techniques that detects decomposition of hybrid Perovskite films to PbI_2 and assists in developing methods to stop the degradation of Perovskite films.

Fontane et al [39] detected secondary phases in Kesterite semiconductors $Cu_2ZnSnS(e)_4$ an absorber in solar thin films using Resonant Raman spectroscopy.

The presence of secondary phases is a problematic issue for the functioning of numerous advanced compound semiconductors. In Kesterite semiconductors, ZnS (Zinc Sulphide) and MoS_2 (Molybdenum Sulphide) act as a secondary phase [39].

Fontane et al [39] excited Kesterite semiconductor materials at various depths at 325 nm excitation wavelength and recorded the Raman spectra. Two peaks at 350 cm^{-1} and 700 cm^{-1} were seen, which were identified as 1st phase ZnS and 2nd phase ZnS, and at 287 cm^{-1} and 408 cm^{-1} were identified as MoS_2 secondary phases [38].

Fontane et al [39] demonstrated that Resonant Raman spectroscopy can detect those secondary phases in crystalline semiconductors that cannot be detected by X-ray diffraction. Avoiding secondary phases is crucial for better performance of solar cells.

5. Conclusions:

Raman spectroscopy is extensively used in the development of solar cells. Raman spectra can detect defects, connecting points in silicon, stability of Perovskites, and other materials used in solar cells, where XRD and other techniques cannot reach. This was exhibited in all the citations mentioned in this chapter. Raman spectroscopy is developing into a quantitative technique for the determination of the chemical composition and structure of materials used in solar cells. In the present chapter, an attempt is made to cover the usefulness of Raman spectroscopy in the development of solar cells.

6. Conflict of Interest: The author declares no conflict of interest

7. Funding: This work is self-financed.

8. Acknowledgement: My special thanks to my son Pranav Rao for his valuable inputs in language improvement.

9. References:

[1]: Website**:** https://www.energy.gov/eere/solar/crystalline-silicon-photovoltaics-research

[2]: Website: https://en.wikipedia.org/wiki/Solar_cell

[3]: Website: https://www.perovskite-info.com/introduction

[4]: M.L. Lai, T.Y.S. Tay, A. Sadhanala, S.E. Dutton, G. Li, R.H. Friend, Z.K. Tan, Tunable Near-Infrared Luminescence in Tin Halide Perovskite Devices, J.Phys.Chem. Lett, 2016, 7, 2653-2658. http://dx.doi.org/10.1021/acs.jpclett.6b01047

[5]: Y. Yu, J. Xia, Y. Yang, Basic Understanding of Perovskite solar cells and passivation mechanism, AIP Advances,2022, 12, 055307. https://doi.org/10.1063/5.0058441

[6]: S. Rahman, A. Haleem, M. Siddiq, M.K. Hussain, S. Qamar, S. Hameedd, M. Waris, Research on dye sensitized solar cells: Recent advancement toward the various constituents of dye sensitized solar cells for efficiency enhancement and future prospects, RSC Adv., 2023, 13, 19508. https://doi.org/10.1039/D3RA00903C

[7]: S. K. Kolekar, R. Ahir, K. Diwate, H. Borate, Synthesis and Characterization of CZTS Thin Films for Solar Cell Applications Published: 05 February 2025, DOI: 10.5772/intechopen.1008712 as part of chapter in the book titled: Innovations in Perovskite Solar Cell Materials and Devices - Cutting-Edge Research and Practical Applications, INTECH (https://www.intechopen.com/chapters/1191070#

[8]: M.Jiang, X.Yan, Cu2ZnSnS4 Thin film solar cells:Present status and Future Prospects, Published:06 March 2013, DOI: 10.5772/50702 as a Part of Book titled: Solar cells-Research and Application Perspectives, INTECH (https://www.intechopen.com/chapters/37686#)

[9]: H.Li, W.Zhang, Perovskite Tandem solar cells: From fundamentals to commercial deployment, Chem.Rev, 2020, 120(18), 9835-9950 (https://doi.org/10.1021/acs.chemrev.9b00780)

[10]: Website**: https://www.perovskite-info.com/perovskitesilicon-tandem-solar-cell-achieves-record-efficiency**

[11]: Y.Zhou, T.Xu, M.Xu, Y.Yin, Y.Wang, Y.Jin, C.Wang, Raman spectroscopy real time detection for the performance of Perovskite solar cell, Optical Materials, 2021,112, 110806 (https://doi.org/10.1016/j.optmat.2021.110806)

[12]: C. Droz, E. Vallat-Sauvain, J. Bailat, L. Fietknecht, J. Meier, A. Shah, Relationship between Raman crystallinity and open-circuit voltage in microcrystalline silicon solar cells Solar Energy Materials and Solar cells, 2004, 8(1), 61-71, https://doi.org/10.1016/j.solmat.2003.07.004

[13]: D.N. Sathyanarayana, Raman Spectroscopy In: Vibrational Spectroscopy: Theory and Applications 3rd edition by D.N. Sathyanarayana, New Age International Publications.

[14]: Voudoukis, N.F. Raman Spectroscopy and Innovative Solar cells – Optical Characterization of Molecules, European Journal of Electrical Engineering and Computer Science. 2019, 3(1), 1-6. . http://dx.doi.org/10.24018/ejers.2019.3.2.67D

[15]: Y.C. Cho, S.I. Ahn, Fabricating a Raman spectrometer using an optical pickup unit and pulsed power, Scientific Reports, 2020, 10(1), 2020, **https://doi.org/10.1038/s41598-020-68650-7**

[16]: N. Tarcea, T. Frosch, P. Roesch, M. Hilchenbach, T. Stuffler, S. Hofer, H. Thiele, R. Hochleitner, J. Popp, Raman spectroscopy A powerful tool for in situ Planetary Science, Space Science Review, 2008, 135. 281-292 https://doi.org/10.1007/s11214-007-9279-y

[17]: R.A. Crocombe, B.W. Kammrath, P.E. Leary, Portable Raman Spectrometers: how small can they get? Spectroscopy supplements, Raman technology for today's spectroscopists, 2023, 38(S6), 32-40. https://doi.org/10.56530/spectroscopy.cn5172t4

[18]: M. Dimitrievska, F. Olivia, M. Guc, S. Giraldo, E. Saucedo, A. Perez-Rodriguez, V.I.Roca, Defect characterization in Cu2ZnSnSe4 kesterites via Resonance Raman spectroscopy and the impact on optoelectronic solar cell properties, J. Mater.Chem. A, 2019, 7, 13293-13304. https://doi.org/10.1039/C9TA03625C

[19]: S.Bienz, G.Spaggiari, D.Calestani, G.Trevisi, D.Bersani, R.Zenobi, N.Kumar, Nanoscale Chemical Analysis of thin film solar cell interfaces using Tip-Enhanced Raman Spectroscopy, ACS Applied Materials and Interfaces, 2024, 16(12), 14704-14711, https://doi.org/10.1021/acsami.3c17115

[20]: L.Shaowei, L.Yanping, Y.Rongxing, L.Liwei, Q.Junie, Coherent Anti-Stokes Raman scattering Microscopy and its applications, Frontiers in Physics, 2020, 8, 598420, https://doi.org/10.3389/fphy.2020.598420

[21]: G. Sarau, R. Lewandowska, A. Bochmann, S. Christiansen, From Micro- to Macro- Raman Spectroscopy: Solar Silicon for a case study Chapter 8 in Book: Advanced Aspects of Spectroscopy, INTECH, 2012, 221-246, https://www.intechopen.com/chapters/38553#:~:text=29%20August%202012-,DOI%3A%2010.5772/48160,-IntechOpenDOI:10.5772/48160

[22]: Website: https://optosky.com/Raman-spectroscopy-in-Photovoltaic-Materials-Research.html

[23]: J. Y. Kim, J.W Lee, H.S. Jung, H. Shin, N.G. Park, High efficiency Perovskite Solar cells, Chem.Rev, 2020, 120, 7867-7918, https://doi.org/10.1021/acs.chemrev.0c00107

[24]: M.A. Green, A.H. Baille, H.J. Snaith, The emergence of Perovskite Solar Cells, Nature Photonics, 2014,.8, 506-514, https://www.nature.com/articles/nphoton.2014.134

[25]: Y. Chen, M. Zhang, F. Li, Z. Yang, Recent Progress in Perovskite Solar cells: Status and Future, Coatings, 2023, 13(3), 644. https://doi.org/10.3390/coatings13030644

[26]: C. Quarti, G. Grancini, E. Mosconi, P. Bruno, J.M. Ball, M.H. Lee, H.J. Snaith, A. Petroza, F.D. Angelis, The Raman Spectrum of the $CH_3NH_3PbI_3$ hybrid perovskite: Interplay of theory and experiment, J.Phys.Chem. Lett, 2014, 5(2), 279-284, https://doi.org/10.1021/jz402589q

[27]: P. Nandi, C. Giri, B. Joseph, S. Rath, U. Manju, D. Topwal, $CH_3NH_3PbI_3$, A Potential Solar cell candidate: Structural and Spectroscopic Investigation, J. Phys.Chem. A, 2016, 120, 9732-9739 https://doi.org/10.1021/acs.jpca.6b09718

[28]: S. Ruan, D.P. Meekin, R. Fan, N.A.S. Webster, H.E. Heidepriem, Y.B. Cheng, J. Lu, Y. Ruan, C.R.McNeill, Raman spectroscopy of Formamidinium based Lead halide Perovskite single crystals, J.Phys.Chem.C, **2020,** 124 (4), 2265-227 http://dx.doi.org/10.1021/acs.jpcc.9b08917

[29]: K. Gjorgjeviky, M. Bukleski, S. Dimitroveka-Lazova, S. Aleksovska, Raman spectroscopy as a tool for predicting the dimensionality and octahedra connectivity in lead iodide perovskites, Journal of Molecular structure, 5 Dec 2023, 1293, 136236 https://doi.org/10.1016/j.molstruc.2023.136236

[30]: M.Shahbazi, H.Wang, Progress in research on the stability of organometal perovskite solar cells. Solar energy, 2016, 123, 74-87.

[31]: Z.Q.Yu, R.B.H. Tan, Anti solvent crystallization, Crystals, 2020, 10(9), 748. https://doi.org/10.3390/cryst10090748

[32]:K.E.A. Hooper, H.K.H.Lee, M.J.Newmann, S.Meroni, J.Baker, T.M.Watson, W.C.Tsoi, Probing the degradation and homogeneity of embedded perovskite semiconducting layers in photovoltaic devices by Raman spectroscopy, Phys.Chem.Chem.Phys, 2017, 19, 5246-5253, https://doi.org/10.1039/C6CP05123E

[33]: Website**:** https://www.edinst.com/blog/mapping-the-raman-spectra/,

[34]: S. Ghosh, D. Rana, B. Pradhan, P. Donfack, J. Hofkens, A. Materny, Raman spectroscopy of Formamidinium-Based Lead mixed halide perovskite bulk crystals, ChemPhysChem, 2023, 24, e202300303.

[35]: P. Pistor, A. Ruiz, A. Cabot, V.I. Roca, Advanced Raman spectroscopy of methylammonium lead iodide: Development of a Non-Destructive characterization methodology, Sci Rep 2016, 3, 35973, https://doi.org/10.1038/srep35973

[36]: M. Ledinsky, P. Lopez, B. Niesen, J. Holovsky, S.J. Moon, J.H. Yum, S.D. Wolf, A. Fejfar, C. Ballif, Raman spectroscopy of organic-inorganic halide Perovskites, J.Phys.Chem. Lett, 2015, 6, 401-406. https://doi.org/10.1021/jz5026323

[37]: R. Gottesman, L. Gouda, B.S. Kalanoor, E. Haltzi, S. Tirosh, E.R. Hodesh, Y. Tischler, A. Zaban, C. Quarti, E. Mosconi, F.D. Angelis, Photoinduced Reversible Structural Transformation in free-standing $CH_3NH_3PbI_3$ Perovskite films. J.Phys.Chem.Lett, 2015, 6(12), 2332-2338. https://doi.org/10.1021/acs.jpclett.5b00994

[38]: Qiong Chen, Henan Liu, Hui-Seon Kim, Yucheng Liu, Mengjin Yang, Naili Yue, Gang Ren,Kai Zhu, Shengzhong Liu, Nam-Gyu Park, and Yong Zhang, Multiple-Stage Structure Transformation of Organic-Inorganic Hybrid Perovskite CH3NH3PbI3. PHYSICAL REVIEW X 6, 031042 (2016). https://journals.aps.org/prx/abstract/10.1103/PhysRevX.6.031042

[39]: X.Fontane, L.C.Barrio, V.I.Roca, E.Saucedo, A.P.Rodriguez, J.R.Morante, D.M.Berg, P.J.Dale, S.Siebntritt, In-depth resolved Raman scattering analysis for the identification of secondary phases: characterization of Cu_2ZnSnS_4 layers for solar cell applications, Applied Physics letters, 2011, 98, 181905, https://doi.org/10.1063/1.3587614